Available online at www.sciencedirect.com
ScienceDirect
Geochimica et Cosmochimica Acta 70 (2006) 4287–4294
Geochimica
www.elsevier.com/locate/gca

Europium isotopic variations in Allende CAIs and the nature of mass-dependent fractionation in the solar nebula

Frédéric Moynier [a,*], Audrey Bouvier [a], Janne Blichert-Toft [a], Philippe Telouk [a], Daniela Gasperini [b], Francis Albarède [a]

[a] *Laboratoire de Sciences de la Terre, Ecole Normale Supérieure de Lyon, 46 allée d'Italie, 69364 Lyon, France*
[b] *Dipartimento di Scienze della Terra, Università di Pisa, 53 via S. Maria, 56126 Pisa, Italy*

Received 20 February 2006; accepted in revised form 19 June 2006

Abstract

We measured the $^{153}Eu/^{151}Eu$ ratio by MC-ICP-MS for a terrestrial basalt, two terrestrial soils, and four meteorites (whole rocks and/or chondrules of Bjurböle, Forest City, Murchison, and Allende) and found no isotopic variations. By contrast, two CAI separates from two different pieces of Allende show a ^{153}Eu deficit of up to one per mil. Such a shortage in the heavy isotopes, which had also been identified in Allende CAIs for Sr [Patchett, P.J. 1980b. Sr isotopic fractionation in Allende chondrules: a reflection of solar nebular processes. *Earth Planet. Sci. Lett.* **50**, 181–188], cannot reflect evaporative fractionation. The lack of Sm isotope fractionation in the same samples further makes fractionation by purely kinetic processes an unlikely cause of the anomalous Eu isotopic composition. An alternative interpretation is condensation from a vapor already significantly depleted in Eu, but in such a scenario the fate of the missing material is unclear. We therefore prefer yet another interpretation, based on the low ionization potential of Eu (and Sr), in which electromagnetic separation of the ionized gas preferentially depletes the nebular gas in heavy isotopes.

1. Introduction

The isotopic variability of the elements in the Solar System results from a number of different processes. Most commonly, vibrational energy partitioning between coexisting phases at equilibrium or at kinetic conditions leads to mass-dependent isotope fractionation. With a few exceptions, the amplitude of these effects is most noticeable for light elements. A major challenge in isotope geochemistry is to disentangle the mass bias created by the analytical procedure from natural mass fractionation. Other processes are non-mass-dependent in nature, in particular the ^{16}O enrichment in refractory inclusions of chondrites, which has so far eluded a consensual explanation (Thiemens, 1999; McKeegan and Leshin, 2001; Clayton, 2003). Ingrowth of isotopic excesses upon decay of radioactive isotopes, both long-lived (e.g., ^{87}Rb–^{87}Sr) and short-lived (e.g., ^{26}Al–^{26}Mg), and spallation by cosmic rays during the wandering of meteorites through space are examples of other mass-independent fractionation processes. A different type of isotopic anomaly observed for non-radiogenic stable isotopes is inherited from nucleosynthesis and attests to incomplete mixing in the solar nebula. This is particularly interesting for Eu, which is largely an *r*-process element and for which an optical determination of the isotopic composition is available from old, low-metallicity stars (Aoki et al., 2003). The presence of non-mass-dependent anomalies is demonstrated by first assessing mass-dependent fractionation, which so far has required that the element under consideration possesses at least three stable isotopes, each unaffected by non-mass-dependent processes. However, since the advent of multiple collector, inductively-coupled plasma mass spectrometry (MC-ICP-MS), the analytical mass-dependent bias can now be controlled for elements with only two isotopes, such as Cu, which consists of the isotopes 63 and 65: today Cu

* Corresponding author.
E-mail address: fmoynier@ens-lyon.fr (F. Moynier).

0016-7037/$ - see front matter © 2006 Elsevier Inc. All rights reserved.
doi:10.1016/j.gca.2006.06.1371

isotopic compositions are routinely measured (Maréchal et al., 1999), but whether Cu isotopic variability is produced by mass-dependent fractionation or results from some other process is still unclear (Luck et al., 2003). Here, we report the isotopic composition of Eu, which has two isotopes, ^{151}Eu and ^{153}Eu, on a small number of samples of terrestrial and extra-terrestrial origin. The natural abundances of the two isotopes (^{153}Eu/^{151}Eu = 1.0916) are currently known to a precision of ~1 per mil and, so far, no isotopic variation has been observed (Chang et al., 1994). We confirm that natural Eu isotopic variability in terrestrial samples and meteorites is well within the improved analytical uncertainties obtained by MC-ICP-MS, but that a prominent anomaly is observed for some Allende refractory inclusions.

2. Samples and analytical methods

We analyzed three terrestrial samples, a basalt from the Piton des Neiges (Réunion Island) and two soils collected next to Manosque (Southeastern France). We also measured the whole-rocks of three chondrites, Allende (CV3), Murchison (CM2), and Bjurböle (L/LL4), and populations of separated chondrules from Bjurböle and Forest City (H5). We finally analyzed populations of separated CAIs from Murchison and Allende, as well as a single CAI inclusion from Allende (sample USNM 3529-31), which is a type B inclusion with a group I rare-earth element (REE) pattern (Mason and Martin, 1977).

For terrestrial materials and bulk meteorites, we digested 1–2 g of sample in a concentrated HF–HNO_3 mixture using PFA Savillex beakers placed inside a steel-jacketed metal container at 140 °C for 48 h. We also retrieved samples that had been previously processed for Pb separation. For these, 0.4–0.8 g of chondrules and 0.2–0.4 g of CAIs had been hand-picked, leached, dissolved (in a ~ 10:1 mixture of concentrated HF–HNO_3 in steel-jacketed PTFE bombs at 150 °C for 1 week), and the final sample solutions run through an anion-exchange resin (AG1-X8, 200–400 mesh) in HBr medium, which absorbs Pb while the major elements and REEs pass straight through. The combined major element and REE fraction was collected and subsequently processed for Eu separation. Inclusion USNM 3529-31 (0.15 g) likewise was dissolved in a ~10:1 mixture of concentrated HF–HNO_3 in a steel-jacketed teflon bomb at 150 °C for 1 week. To achieve complete sample dissolution in 6 M HCl, the sample was treated with $HClO_4$ to decompose the fluorides formed during the initial attack. The resulting perchlorates in turn were driven off with 6 M HCl. This sample was taken directly through the Eu separation protocol without any preceding Pb chemistry. To separate Eu, the light REEs were first purified from the bulk sample matrix on a cation exchange resin (AG50W-X8, 200–400 mesh) in HCl medium. Europium was then isolated from most of the other light REEs by reversed-phase extraction chromatography on HDEHP-coated fluoropolymer beads (Alltech T-Port-F, 80–100 mesh), also in HCl medium. In order to ensure complete yield for Eu, to avoid mass fractionation on the column, about half the Sm and Gd of the samples together with traces of Nd (due to the HDEHP tailing effect) were eluted with the Eu fraction. The natural Sm thus present in the Eu separates was later used for the correction of mass fractionation during mass spectrometric analysis. The total procedural blank was better than 40 pg Eu.

All the samples except one, USNM 3529-31, were analyzed on the VG Plasma 54 MC-ICP-MS at ENS Lyon. Sample USNM 3529-31 was analyzed on both the Plasma 54 and the new Nu Plasma 500 HR at ENS Lyon. The nine Faraday cups were positioned to collect masses 146, 147, 149, 150, 151, 152, 153, 154, and 157 on the VG Plasma 54 and masses 145, 147, 149, 150, 151, 152, 153, 154, 155, and 157 on the Nu Plasma 500 HR, which leaves out mass 148 on both instruments. Measuring ^{148}Sm, a shielded *s* nuclide, would have provided a useful additional stable isotope ratio for verification of the respective contribution of *s* and *r* processes. However, not enough collectors (9) were available on the Plasma 54, while the ion beam array on the Nu Plasma (controlled by the 'zoom lens') was incompatible with the positioning of a collector at mass 148 without sacrificing one of the other masses, all of which were mandatory for the present analysis scheme. The accurate measurement of the isotopic composition of Eu, has, like other elements with only two isotopes (Maréchal et al., 1999), greatly benefited from the advent of MC-ICP-MS, in that the analytical mass bias with this technique can be monitored in two ways, first by bracketing each sample with standards and second by analyzing a different element used as an external spike, in this case Sm.

2.1. Sm isotopic analysis

Sm isotopic abundances were determined by standard bracketing. They were corrected for Nd and Gd isobaric interferences on masses 150, 152, and 154 by measuring the abundances of masses 146 (145 on the Nu Plasma) and 157, respectively, and using the following isotopic ratios: ^{150}Nd/^{146}Nd = 0.32749, ^{150}Nd/^{145}Nd = 0.67855, ^{152}Gd/^{157}Gd = 0.01278, and ^{154}Gd/^{157}Gd = 0.13930. By assessing the mass bias with respect to a standard solution (JMC batch # 0-1497L and ^{149}Sm/^{147}Sm = 0.92160) at each mass, this procedure allowed us to identify which isotopes are free from nucleosynthetic effects. Comparison of the data obtained on USNM 3529-31 shows errors on the standard bracketing technique on the order of 2 to 3×10^{-4} units per amu. Table 1 lists the repeated measurements of a 1:1 mixture of Sm and Eu standard solutions for different cuts of Sm on the HDEHP column (the only step for which recovery may not be quantitative). The data clearly demonstrates that the separation yield does not affect the Sm isotopic compositions. Even with up to 80% loss of Sm, the results remain within the uncertainties of standard bracketing.

Table 1
Isotopic compositions of Sm and Eu in the different fractions collected during HDEHP elution for different Sm cuts

% Sm collected with Eu	$\varepsilon^{147/154}$Sm/(−7)	$\varepsilon^{149/154}$Sm/(−5)	$\varepsilon^{150/154}$Sm/(−4)	$\varepsilon^{152/154}$Sm/(−2)	$\varepsilon^{153/151}$Eu/(2)	Eu/Sm
100%	0.6	0.6	0.9	0.5	−0.1	1
35%	0.5	0.5	−0.1	0.6	−0.9	3
Re-run	0.5	0.6	1.2	0.9	−0.5	3
20%	−0.2	−0.2	−4.1	0.5	−1.0	5
Re-run	0.2	0.4	0.9	0.0	0.3	5

2.2. Eu isotopic analysis

The instrumental mass fractionation of Eu for each sample was estimated using the anomaly-free ^{149}Sm/^{147}Sm ratio (McCulloch and Wasserburg, 1978a) of the sample and the bracketing standards for internal normalization and an exponential law of mass fractionation. This procedure, adapted from Maréchal et al. (1999) for Cu and Zn isotope analysis and from Blichert-Toft et al. (2002) for Lu and Yb isotope analysis, assumes that isotope fractionation of Sm and Eu during chemical processing remains very small and correlated by the law of mass dependence. This assumption is amply justified by both the replicate analyses reported in Table 1, for which the variable proportions of Sm deliberately lost during the separation protocol show no resolvable effect on Eu isotope compositions, and the excellent reproducibility of the ^{153}Eu/^{151}Eu ratio for all the non-CAI samples. For the standard, the Eu mass bias was assumed to be identical to that of Sm. The isotopic shift was evaluated by comparing the mass-fractionation-corrected ^{153}Eu/^{151}Eu ratios of the sample and the bracketing standards. The standard used to bracket the samples was a JMC Eu solution (batch # 804.46A), which was prepared intentionally to have a Eu concentration similar to that of the sample solutions. The external reproducibility of each sample isotope ratio, as estimated from six replicate analyses of the basaltic sample included in this study, was 50×10^{-6} units per amu at the 2σ level.

We checked the mass spectrum for possible interferences with molecular ions, in particular Ba (^{135}Ba/^{16}O, ^{137}Ba/^{16}O), La (^{139}La/^{12}C), and Cd (^{111}Cd/^{40}Ar, ^{113}Cd/^{40}Ar). The Cd and La signals were found to be negligible (Cd/Eu and La/Eu $< 10^{-6}$) after the Eu purification chemistry. By contrast, a small Ba signal could be detected, in particularly for the CAI samples, with a ^{151}Eu/^{135}Ba ratio of ~4500. Using a plot of ^{153}Eu/^{151}Eu vs ^{152}Sm/^{150}Sm or ^{154}Sm/^{152}Sm (Fig. 1) we show, however, that the contribution of BaO on the Eu signal can be disregarded: BaO would interfere with masses 150–154 and a mixing curve between ^{153}Eu/^{151}Eu and ^{152}Sm/^{150}Sm on the one hand and ^{153}Eu/^{151}Eu and ^{154}Sm/^{152}Sm on the other hand can be calculated between the pure Eu + Sm end-member and the hypothetical composition for which all the Ba present in the analysis would be oxidized. The mixing curve clearly deviates from the data. In addition, a BaO contribution would *increase* the 153/151 ratio, which is not what the present results show. We therefore conclude that isobaric interferences of BaO on Eu can be ignored.

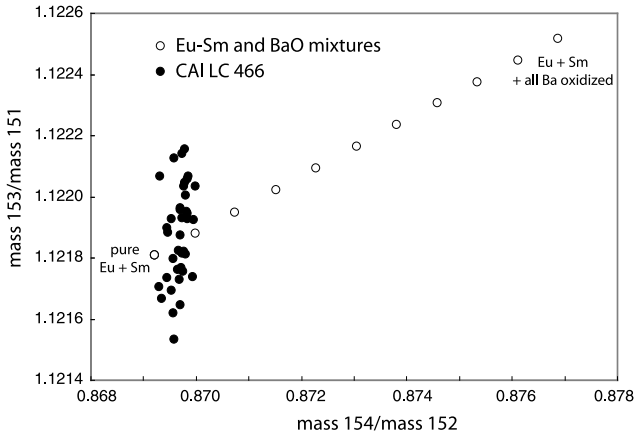

Fig. 1. Graph of measured ^{153}Eu/^{151}Eu and ^{154}Sm/^{152}Sm for UCLA CAI sample LC 466 (solid symbols). Each point represents a different cycle. The open symbols represent the mixing curve between metallic Eu + Sm (left) and Eu + Sm + BaO (right) with BaO corresponding to the total Ba present in the analysis. The deviation of this curve from the data points indicates that BaO does not contribute to the Eu signal.

3. Results

The isotopic abundances are reported in Table 2. Isotopic ratios are expressed as relative deviations from the standard in parts per 10,000 (ε):

$$\varepsilon^{n/m}X = \left[\frac{({}^{n}X/{}^{m}X)_{\text{sample}}}{({}^{n}X/{}^{m}X)_{\text{standard}}} - 1\right] \times 10^{4} \quad (1)$$

divided by the mass difference, where X stands for either Eu or Sm. For $X =$ Eu, $n = 153$ and $m = 151$. For $X =$ Sm, n represents either of the masses 147, 149, 150, 152 and $m = 154$.

The isotopic compositions of Sm are constant to within 2–3 ε/amu, which is close to the external reproducibility. These results are not as reproducible as those obtained for Eu (see below), which we ascribe to plasma conditions being relatively unsteady, in particular on the Plasma 54. When the $\varepsilon^{n/m}$Sm values are divided by the corresponding mass difference, a constant number is in general obtained, which suggests that no nucleosynthetic anomaly is present in the Sm of the present samples. The measurements involving mass 150 are of inferior reproducibility, which we suspect results from a significant Nd interference correction (Nd/Sm ~ 10^{-2}). We nevertheless conclude that the variations in the relative abundances of masses 147, 149, and 154 in the present samples are largely accounted for by the instrumental mass bias. This is also likely to be

Table 2
Isotopic compositions of Sm and Eu in chondrules, CAIs, bulk rocks of chondrites, a Réunion basalt, and terrestrial soils

Sample ID	Type	$\varepsilon^{147/154}$ Sm/(−7)[c]	$\varepsilon^{149/154}$ Sm/(−5)[c]	$\varepsilon^{150/154}$ Sm/(−4)[c]	$\varepsilon^{152/154}$ Sm/(−2)[c]	$\varepsilon^{153/151}$ Eu/(+2)[c]	$\varepsilon^{153/151}$ Eu/(+2)[d]
Forest City MNHN 987chondrules	H5	1.7	1.2	1.4	0.9	0.2	−1.5
BjurböleMNHN 1672 & 2493 whole-rock	L/LL4	2.3	2.3	0.2	−1.5	2.4	−1.3
Bjurböle MNHN 1672 & 2493 chondrules	L/LL4	2.7	3.9	1.3	1.5	1.2	−0.8
Replicate[a]	L/LL4	2.9	3.2	1.6	0.7	2.2	−0.9
Murchison Chicago ME 2644 whole-rock	CM2	2.9	2.8	3.2	6.7	−2.7	−1.9
Allende MNHN 3181 whole-rock	CV3	−0.1	−0.2	6.5	3.9	1.2	−2.6
Murchison Chicago ME 264 CAI	CM2	−1.1	−1.2	−2.6	−0.8	−1.4	−0.6
Allende UCLA LC 466 CAI	CV3	3.0	3.0	1.4	2.8	−1.4	−3.9
Allende MNHN 3181 CAI	CV3	2.4	2.3	0.8	3.0	−3.2	−5.5
Re-run	CV3	2.0	2.2	1.1	1.1	−4.4	−5.9
Allende USNM 3529-31 CAI NU 500	CV3	1.1	1.2	−2.3	1.2	−2.5	−1.3
Allende USNM 3529-31 CAI Plasma 54	CV3	−1.2	−1.2	−5.1	−1.8	−1.8	−0.8
PN (Piton des Neiges)[a]							
Separation 1	Basalt	2.2	2.2	1.9	2.0	3.4	−1.0
Separation 2		0.2	0.3	−0.2	0.4	5.8	−0.9
Separation 3		3.9	3.7	3.4	3.0	−1.8	−0.8
Separation 4		−0.1	−0.1	−0.3	0.0	4.9	−1.4
Separation 5		−1.1	−1.2	−3.0	−1.6	−4.1	−0.8
Separation 6		0.1	0.1	−0.1	0.1	−1.1	−0.6
S1[b]							
Digestion 1 separation 1	Soil	−3.1	−3.1	−3.2	−2.7	−1.0	−1.2
Digestion 1 separation 2		−0.1	−0.2	−0.4	0.2	−0.4	−1.2
Digestion 2 separation 1		0.0	0.0	0.0	0.3	−0.6	−1.0
Digestion 2 separation 2		0.0	0.0	0.0	0.2	−0.5	−0.8
S2[a]							
Digestion 1 separation 1	Soil	0.4	0.3	0.3	0.6	0.0	−1.1
Digestion 1 separation 2		−0.5	−0.7	−0.7	−0.4	−0.2	−2.0

[a] One single sample digestion followed by chemical separation on liquid aliquots.
[b] Two separate sample digestions each followed by chemical separation on liquid aliquots.
[c] Standard-sample bracketing.
[d] Analytical bias corrected using the $^{149}Sm/^{147}Sm$ in the same fraction.

the case, although with larger errors, for mass 152. There is no evidence that any particular variety of sample (basalts, soils, or meteorites) is affected by significant Sm isotope variations.

On average, the measured $^{153}Eu/^{151}Eu$ ratio of the terrestrial samples consistently deviates from the standard by about −1 ε/amu, which strongly suggests that the Eu standard we used was preferentially enriched in ^{153}Eu during manufacturing with respect to the Bulk Earth value. The six replicates of the Piton des Neiges basalt and the terrestrial soils are in good agreement. Fig. 2 compares the isotopic abundances of Eu for the different samples. The values for the terrestrial samples, the chondrules, and the bulk meteorites are all within error of the mean ε/amu value of −1. These results confirm that Sm can be used efficiently to correct for instrumental mass bias and that chemical separation introduces only very little, if any, isotope fractionation. By contrast, the ^{153}Eu deficit is substantial for both the Allende CAI MNHN 3181 (−5.5 and −5.9 ε/amu) and the Allende CAI UCLA LC 466 (−3.9 ε/amu). However, while these two samples each carry a significant Eu anomaly, there is no indication of their Sm being anomalous as well. The largest Eu isotopic anomaly observed in the CAIs with respect to common terrestrial and meteoritic material thus is −5.9 ε/amu. By contrast,

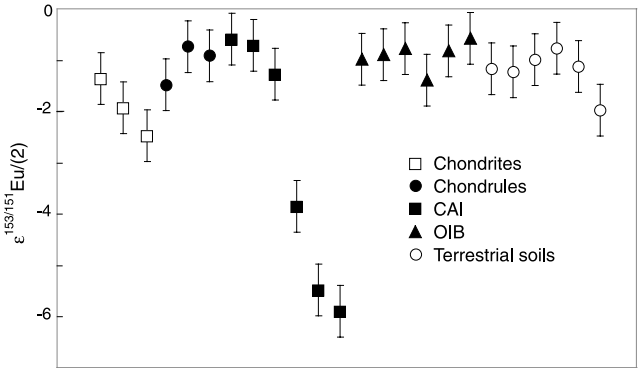

Fig. 2. Eu isotopic data for CAIs, chondrules, a terrestrial basalt, and two terrestrial soils.

the Murchison CAIs and the single Allende CAI USNM 3529-31 all appear to be devoid of any significant anomalies. The $^{153}Eu/^{151}Eu$ ratios of USNM 3529-31 measured on both the Plasma 54 (−0.8/amu) and the Nu Plasma (−1.3/amu) are in agreement within error bars.

4. Discussion

The $^{153}Eu/^{151}Eu$ ratio of the terrestrial samples, bulk meteorites, and chondrules show no variability outside of

analytical error bars, which points to an overall lack of fractionation by geological processes. This is exactly what is to be expected from the small relative mass difference between the two Eu isotopes and the insoluble character of REEs, which are averse to pervasive mobility. The enrichment in the *light* Eu isotope of two of the Allende CAIs (the MNHN and the UCLA samples) measured here, however, is puzzling, but strikingly reminiscent of the enrichment of the light stable isotope of Sr observed in Allende CAIs (Patchett, 1980a) and chondrules (Patchett, 1980b). Europium from the single CAI inclusion USNM 3529-31 and the Murchison CAIs is isotopically normal, or nearly normal, which suggests that the contrast between type B (restricted to CV) and type A is not sufficient to account for a difference between Murchison and Allende. The isotopic anomalies therefore seem to be carried by particular objects, especially in Allende in which inclusions are known for their large diversity (Grossman, 1975). We will now examine some of the possible interpretations of a ^{151}Eu excess.

4.1. Short half-life radioactivities

We consider spallation by cosmic rays over 4.5 Gy to be an unlikely explanation because the effects should be equally visible in both the matrix and the refractory inclusions. Luck et al. (2003) discussed a correlation between ^{63}Cu/^{65}Cu and Ni/Cu in bulk chondrites and suggested that it may reflect the presence of the decay products of ^{63}Ni ($T_{1/2} = 100$ y). Likewise, ^{151}Eu excesses in CAIs may be inherited from the decay of ^{151}Sm ($T_{1/2} = 90$ y). In both cases, an improbable explanation is that the anomalous material formed while the parent nuclides ^{63}Ni and ^{151}Sm were still extant. Alternatively, the progenitor may have been produced upon irradiation of silicates by particles sufficiently energetic (>6 MeV) to detach nucleons. Such highly energetic particles are, however, difficult to produce in significant quantities in the nascent Sun.

4.2. Nucleosynthetic effects

Isotopic anomalies in Ba, Nd, and Sm observed in a FUN inclusion have been interpreted as an excess of *r*- relative to *s*-process nuclides (Clayton, 1978; McCulloch and Wasserburg, 1978a,b). Europium is one of the elements with the strongest *r* contribution with about 95% of each isotope being produced by *r* processes (Arlandini et al., 1999). Very old stars with low metallicity ([Fe/H] $\leqslant$ 2.5), which are expected to have recorded a smaller number of nucleosynthetic events than the Solar System material, have almost the same *r*-process nuclide abundances (Cohen et al., 2003). More specifically, Aoki et al. (2003) measured the ^{153}Eu/^{151}Eu ratio of one of these stars (CS 31082-001) using the hyperfine structure of its spectrum and found that it agreed, within errors, with those of other *r*-process-enhanced objects, as well as with that of the canonical abundances of the Solar System. It is therefore unlikely that the anomalies observed in the present study reflect a variable contribution from different *r*-processes. It is also unlikely that the CAIs analyzed here contain a substantial excess of *r*-process nuclides: although ^{154}Sm is more than 99% an *r*-process nuclide, the abundance of this isotope in the samples containing a Eu anomaly shows no identifiable excesses. Finally, we discount the effect of an *s*-process anomaly on the small *s* (<5%) component of Eu on the basis that there is no excess on the pure *s*-process nuclide ^{150}Sm.

4.3. Equilibrium evaporation and condensation

The bearing of REE distributions in Allende CAIs on condensation and volatilization processes has received a great deal of attention (e.g. (Boynton, 1975; Davis and Grossman, 1979; Wang et al., 2001)). These elements clearly demonstrate massive evaporative loss and recondensation during CAI formation and processing (e.g. Wark and Boynton (2001)). The standard isotope fractionation theory (Bigeleisen and Mayer, 1947; Urey, 1947) holds that bonds with a deep and narrow potential well ('stiff' bonds) concentrate the heavy isotopes. Condensed phases therefore usually are isotopically heavier than the coexisting gas phase. From the refractory nature of CAI inclusions, however, it is expected that, as long as the vapor is in equilibrium with the solid surface, the light and not the heavy isotope should be depleted with respect to the ambient vapor, regardless of whether the inclusions are early condensates (Grossman, 1972) or volatilization residues (Chou et al., 1976). Enrichment of the heavy isotopes in the refractory phase has notably been observed for Mg, Si, Ca, and Ti during experimental evaporation of material with solar compositions (Floss et al., 1996; Grossman et al., 2000; Wang et al., 2001).

A deficit in ^{153}Eu is therefore unlikely to be created in a solid residue by evaporation. By contrast, such a deficit could develop by condensation of an isotopically unfractionated vapor phase if the CAIs precipitated only after a substantial fraction of the hot vapor had already been lost from the system (Fig. 3) (late condensates). Assuming that the equilibrium isotope fractionation factor between the solid and the vapor is α, we can write the Rayleigh distillation equation for the condensate as:

$$\left(\frac{^{153}\mathrm{Eu}}{^{151}\mathrm{Eu}}\right)_{\mathrm{cond}} = \alpha\left(\frac{^{153}\mathrm{Eu}}{^{151}\mathrm{Eu}}\right)^{0}_{\mathrm{vap}} F_r^{\alpha-1} \qquad (2)$$

in which the superscript 0 stands for the unfractionated material and F_r for the fraction of initial ^{151}Eu moles left in the vapor. Isotopically light solids start precipitating for fractions F_r of ^{151}Eu precipitated, such as $\alpha\, F_\mathrm{r}^{\alpha-1} = 1$, which is well approximated by $F_\mathrm{r} = \mathrm{e}^{-1/\alpha}$. For isotopic fractionation, α is very close to unity and F_r is essentially independent of the element and equal to $1/e$. Consequently, for all elements, isotope fractionation reversal takes place after ~63% of the element has been removed from the va-

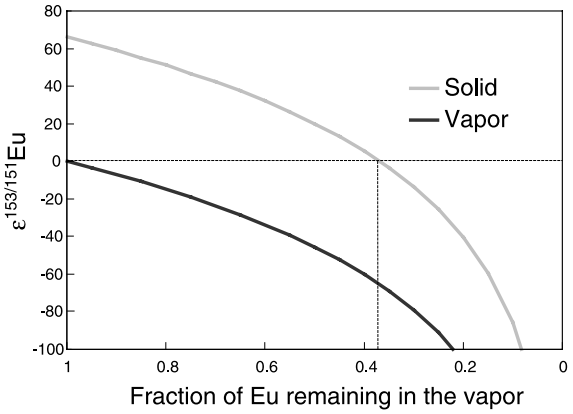

Fig. 3. Calculation of the Rayleigh distillation equation. Isotopically light solids start precipitating after ~63% of the Eu has been removed from the vapor, i.e., for a fraction of Eu remaining of ~37%.

por. How so much isotopically heavy material can be unaccounted for, however, remains unexplained and we therefore seek alternative solutions.

4.4. Kinetic fractionation during incomplete condensation

It has been suggested that isotope fractionation during condensation may result from the different velocities at which isotopes travel in gases (Kehm et al., 2003; Richter, 2004); Patchett (1980a,b) ascribed the enrichment of the light isotopes of Sr in Allende CAIs and chondrules to condensation from a gas kinetically enriched in the lighter isotopes. For the present samples, however, the conspicuous lack of Sm isotope fractionation while Eu is isotopically anomalous, does not favor this explanation and the mere fact that most refractory elements in CAIs are enriched in their heavy isotopes is a strong argument against kinetic isotope fractionation. The contrast between the isotopically light Eu and Sr of CAIs on the one hand and their generally heavy Mg and Si (Clayton et al., 1988) on the other hand provides a similar indication. Richter (2004) considered kinetic effects during the condensation of Mg vapor in the experiments of Uyeda et al. (1991) and concluded that their results "cannot be explained by the standard representation of condensation" given in his comprehensive treatment of evaporation/condensation. As pointed out by Richter (2004), most molecules bounce off the surface of the solid target and a 'sticking' probability must be assumed which could have a strong effect on isotopic fractionation. This author uses a species-dependent sticking coefficient, which he acknowledges should be mass-dependent, to modulate the deposition rates. A simple way of describing the sticking probability is to represent it through the standard equation of thermally activated (Boltzmann) processes as proportional to the residence time τ of the impinging molecules at the surface:

$$\tau \approx \frac{1}{\nu} \exp\left(\frac{\Delta G_{\text{ads}}}{RT}\right). \quad (3)$$

In this equation, the frequency ν measures the number of attempts per unit time made by the molecules to escape the surface sites, while ΔG_{ads} is the free energy of the bond between the molecule and the surface (e.g., Hudson, 1998). For a light isotope, ν should be higher—because vibration frequencies vary with $M^{-1/2}$- and ΔG_{ads} should be less negative—because the stiff bonds of the solid phase concentrate heavy isotopes. Both effects combine to make the residence time at the surface of the solid shorter and hence the sticking coefficients for the lighter isotopes smaller, thus reversing the effect of kinetic fractionation. In the absence of contrary experimental evidence, we therefore conclude that kinetic vapor deposition does not necessarily fractionate the light isotope into the condensed phase. Dauphas and Rouxel (2006) developed a condensation model which takes crystallization into account. This new model portrays a more realistic scenario than did the original kinetic condensation model, but it does not appear to explain the contrast between isotopically fractionated Eu and unfractionated Sm.

4.5. Electromagnetic effects

Magnetic separation in the plasma surrounding the young Sun within ~0.1 AU is a plausible alternative interpretation of such a reversed isotope fractionation. Ionization usually is weak in the solar nebula at temperatures below 1000 °C as it is reduced to the effect of cosmic γ-rays. Thermal ionization quickly becomes extremely important at higher temperatures (Umebayashi, 1983; Gammie, 1996; Balbus and Hawley, 2000). Because K has a particularly low ionization potential and is relatively abundant ($K/H = 1.35 \times 10^{-7}$), this element is the main source of electrons and is fully ionized at ~2000 °C (Umebayashi, 1983), a temperature considered relevant to flash heating events associated with CAI formation (Wark and Boynton, 2001). Although there is considerable uncertainty about the temperature profile in the inner solar nebula (Morfill, 1988; Wood, 2000; Fromang et al., 2002), such a temperature would certainly be attained at ~ 0.06 AU, where Shu et al. (1996) suggested that CAIs originate. In contrast to other REEs, except Yb, Eu is present in the vapor mostly as a metal and not in oxide form (Boynton, 1975), the latter of which is notoriously more difficult to ionize. This contributes to keeping the Eu ionization potential relatively low (Murad and Hildenbrand, 1976). Modern values of the ionization energies compiled by NIST (http://physics.nist.gov/PhysRefData) suggest that the ionization energies of the two elements differ by $\Delta I_P = 1.33$ eV. A simple application of the Saha equation to the ionization ratios gives

$$\frac{\text{Eu}^+}{\text{Eu}} = \frac{\text{K}^+}{\text{K}} \exp\left(-\frac{\Delta I_P}{RT}\right) \quad (4)$$

in which T is the temperature and R the gas constant. Assuming full ionization for K leads to a proportion

of 0.1 % of Eu ionized at $T = 2000$ °C. The ionization potentials of Eu (5.67 eV) and Sr (5.69 eV) are comparable and the two elements should be ionized to similar extents.

Electromagnetic mass separation becomes significant when the dimensionless ratio $L = eBvR^2/GM_{\odot}M$ between Lorentz and the gravity forces maintaining the gas on Keplerian orbits exceeds unity, in which e is the charge of the electron, B the magnetic field, v the ion velocity with respect to the magnetic field, R the orbital radius, G the gravity constant, $M_{\odot}$ the mass of the Sun, and M the mass of the ion under consideration. This fractionation process is clearly mass-dependent. For Eu at 0.1 AU, L is equal to 1×10^6 Bv (SI) and the electromagnetic effect is likely to be fairly strong in a variety of environments. The Lorentz force eBv only acts when ions move with respect to the magnetic field. Ionization of the disk surface by cosmic rays, and, to a much smaller extent, by radioactivity, imposes a strong coupling (frozen field) between the solar magnetic field and the entire disk beyond a fraction of an AU (Gammie, 1996). Shu et al. (1997), however, argued that magnetic coupling between the Sun and the disk fluctuates along the reconnection ring, which then appears as a potential source of velocity anomalies. Alternatively, Hawley and Balbus (1991) suggested that magnetorotational instabilities in a differentially rotating disk create turbulences and therefore velocity gradients in the ionized part of the disk. Regardless of the origin of the velocity field, ions will appear as moving on 'festooned' orbits (magnetic top or Larmor precession) with tighter wiggles for the light isotopes (the radius of the wiggles is given by the standard mass spectrometer equation) (Fig. 4). Collisions may affect electromagnetic sorting, but only in the equatorial plane, where the mean free path is relatively short. Although the actual ion velocity field is undoubtedly complex, the heavier isotopes of the ionized species move on trajectories of lesser curvature and should appear as being preferentially driven off the orbit of the parent neutral atoms and molecules. Electromagnetic separation could therefore turn isotopic variability into a probe of velocity field fluctuations in the solar nebula.

Such an effect is also expected to be particularly strong for K, which is highly volatile and has a low ionization potential, but should be difficult to observe for other elements, which require much larger temperatures to ionize. Because the K concentration level is extremely low in refractory material, there is currently no available isotopic data for this element on Allende CAIs (Humayun and Clayton, 1995). However, with K being both volatile and highly mobile, such isotopic compositions would in any case prove difficult to interpret. Most other elements have higher ionization energies and may not be appropriate for testing the model of electromagnetic separation. Elements other than Eu and Sr, for which electromagnetically-induced mass fractionation could be significant, should be characterized by low ionization potentials and not be amenable to oxidation at nebular conditions. Clearly, Ba and Yb are potential candidates, but a systematic investigation of the stable isotope abundances of these elements is still wanting.

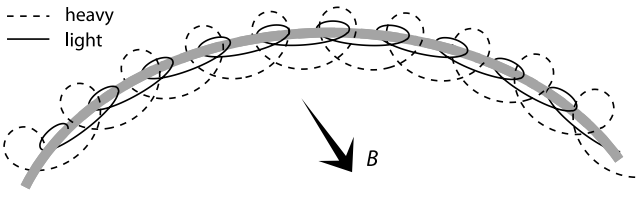

Fig. 4. Cartoon representation of isotope fractionation in the nebular plasma resulting from Larmor precession of ions in orbit around the Sun. Magnetorotational (Balbus-Hawley) instabilities in the magnetic field B drive ions on 'festoons,' whose radii increase with increasing atomic weight.

5. Conclusions

We found that the $^{153}Eu/^{151}Eu$ ratio of terrestrial rocks and meteorites is constant within one ε unit. By contrast, two separates of refractory inclusions from two different samples of Allende each carries a negative Eu anomaly of ~1 per mil. This depletion in the heavy isotope is not of nucleosynthetic origin. If it is a result of preferential evaporation, it would imply that nearly 2/3 of early condensates are unaccounted for, which we consider unlikely. The lack of Sm isotope fractionation in the same samples makes fractionation exclusively by kinetic processes an unlikely cause of the anomalous isotopic composition of Eu. We rather prefer an interpretation that calls on magnetic separation of Eu (and Sr) isotopes within the ionized fraction of the nebular gas.

Acknowledgments

We are particularly grateful to Frank Shu, who attracted our attention to processes in the nebular plasma, and to Thierry Montmerle, who went to great lengths to explain to us as geochemists the mysteries of magnetohydrodynamics effects in the protosolar disk. The help of Chantal Douchet in maintaining the chemistry lab in good working conditions is much appreciated. A.B. is grateful to Jon Patchett for helpful discussions. We also much appreciate insightful feedback from Malcolm McCulloch. We further thank the Programme National de Planétologie (CNRS-CNES) for financial support. We also thank Michèle Bourot-Denise and Brigitte Zanda (Muséum d'Histoire Naturelle de Paris), Alan Rubin (UCLA), and Mini Wadwha (The Field Museum, Chicago) for providing the meteorite samples analyzed in this study. Glen McPherson generously donated the invaluable USNM 3529-31 CAI inclusion. Comments on the manuscript by Nicolas Dauphas, Andy Davis, Klaus Mezger, Mark Rehkämper, and an anonymous reviewer were immensely useful.

Associate editor: Mark Rehkamper

References

Aoki, W., Honda, S., Beers, T.C., Sneden, C., 2003. Measurement of the europium isotope ratio for the extremely metal poor, *r*-process-enhanced star CS 31082-001. *Astrophys. J.* **586**, 506–511.

Arlandini, C., Käppeler, F., Wisshak, K., Gallino, R., Lugaro, M., Busso, M., Straniero, O., 1999. Neutron capture in low-mass asymptotic giant branch stars: cross sections and abundance signatures. *Astrophys. J.* **525**, 886–900.

Balbus, S.A., Hawley, J.F., 2000. Solar Nebula magnetohydrodynamics. *Space Sci. Rev.* **92**, 39–54.

Bigeleisen, J., Mayer, M.G., 1947. Calculation of equilibrium constants for isotopic exchange reactions. *J. Chem. Phys.* **15**, 261–267.

Blichert-Toft, J., Boyet, M., Télouk, P., Albarède, F., 2002. ^{147}Sm–^{143}Nd and ^{176}Lu–^{176}Hf in eucrites and the differentiation of the HED parent body. *Earth Planet. Sci. Lett.* **204**, 167–181.

Boynton, W.V., 1975. Fractionation in the solar nebula—condensation of yttrium and the rare earth elements. *Geochim. Cosmochim. Acta* **39**, 569–584.

Chang, T.L., Qian, Q.-Y., Zhao, M.-T., Wang, J., 1994. The absolute isotopic composition of europium. *Int. J. Mass Spectrosc. Ion Proc.* **139**, 95–102.

Chou, C.-L., Baedecker, P.A., Wasson, J.T., 1976. Allende inclusions: volatile-element distribution and evidence for incomplete volatilization of presolar solids. *Geochim. Cosmochim. Acta* **40**, 85–94.

Clayton, D.D., 1978. An interpretation of special and general isotopic anomalies in *r*-process nuclei. *Astrophys. J.* **224**, 1007–1012.

Clayton, R.N., Hinton, R.W., Davis, A.M., 1988. Isotopic variations in the rock-forming elements in meteorites. *Philos. Trans. R. Soc. A* **325**, 483–501.

Clayton, R.N., 2003. Oxygen isotopes in the Solar System. *Space Sci. Rev.* **106**, 19–32.

Cohen, J.G., Christlieb, N., Qian, Y.Z., Wasserburg, G.J., 2003. Abundance analysis of HE 2148-1247, a star with extremely enhanced neutron capture elements. *Astrophys. J.* **588**, 1082–1098.

Dauphas, N., Rouxel, O., 2006. Mass spectrometry and natural variations of iron isotopes. *Mass Spectrom. Rev.* **25**, 515–550.

Davis, A.M., Grossman, L., 1979. Condensation and fractionation of rare earths in the solar nebula. *Geochim. Cosmochim. Acta* **43**, 1611–1632.

Floss, C., El Goresy, A., Zinner, E., Kransel, G., Rammensee, W., Palme, H., 1996. Elemental and isotopic fractionations produced through evaporation of the Allende CV chondrite: Implications for the origin of HAL-type hibonite inclusions. *Geochim. Cosmochim. Acta* **60**, 1975–1997.

Fromang, S., Terquem, C., Balbus, S.A., 2002. The ionization fraction in alpha models of protoplanetary discs. *Mon. Not. Roy. Astron. Soc.* **329**, 18–28.

Gammie, C.F., 1996. Linear theory of magnetized, viscous, self-gravitating gas disks. *Astrophys. J.* **462**, 725.

Grossman, L., 1972. Condensation in the primitive solar nebula. *Geochim. Cosmochim. Acta* **36**, 597–619.

Grossman, L., 1975. Petrography and mineral chemistry of Ca-rich inclusions in the Allende meteorite. *Geochim. Cosmochim. Acta* **39**, 433–454.

Grossman, L., Ebel, D.S., Simon, S.B., Davis, A.M., Richter, F.M., Parsad, N.M., 2000. Major element chemical and isotopic compositions of refractory inclusions in C3 chondrites: the separate roles of condensation and evaporation. *Geochim. Cosmochim. Acta* **64**, 2879–2894.

Hawley, J.F., Balbus, S.A., 1991. A powerful local shear instability in weakly magnetized disks. II. Nonlinear evolution. *Astrophys. J.* **376**, 223.

Hudson, J.B., 1998. *Surface Science An Introduction*. Wiley, NY, 336p.

Humayun, M., Clayton, R.N., 1995. Potassium isotope cosmochemistry: genetic implication of volatile element depletion. *Geochim. Cosmochim. Acta* **59**, 2131–2148.

Kehm, K., Hauri, E.H., Alexander, C.M.O.D., Carlson, R.W., 2003. High precision iron isotope measurements of meteoritic material by cold plasma ICP-MS. *Geochim. Cosmochim. Acta* **67**, 2879–2891.

Luck, J.M., Othman, D.B., Barrat, J.A., Albarede, F., 2003. Coupled ^{63}Cu and ^{16}O excesses in chondrites. *Geochim. Cosmochim. Acta* **67**, 143–151.

Maréchal, C., Télouk, P., Albarède, F., 1999. Precise analysis of copper and zinc isotopic compositions by plasma-source mass spectrometry. *Chem. Geol.* **156**, 251–273.

Mason, B., Martin, P., 1977. *Smithsonian Contributions to Earth Sciences* **19**, 84–95.

McCulloch, M.T., Wasserburg, G.J., 1978a. More anomalies from the Allende meteorite: samarium. *Geophys. Res. Lett.* **5**, 599–602.

McCulloch, M.T., Wasserburg, G.J., 1978b. Barium and neodymium isotopic anomalies in the Allende meteorite. *Astrophys. J.* **220**, L15–L19.

McKeegan, K.D., Leshin, L.A., 2001. Stable isotope variations in extraterrestrial material. *Rev. Miner. Geochem.* **43**, 279–318.

Morfill, G.E., 1988. Protoplanetary accretion disks with coagulation and evaporation. *Icarus* **75**, 371–379.

Murad, E., Hildenbrand, D.L., 1976. Thermochemical properties of gaseous EuO. *J. Chem. Phys.* **65**, 3250–3256.

Patchett, P.J., 1980a. Sr isotopic fractionation in Ca–Al inclusions from the Allende meteorite. *Nature* **283**, 438–441.

Patchett, P.J., 1980b. Sr isotopic fractionation in Allende chondrules: a reflection of solar nebular processes. *Earth Planet. Sci. Lett.* **50**, 181–188.

Richter, F.M., 2004. Timescales determining the degree of kinetic isotope fractionation by evaporation and condensation. *Geochim. Cosmochim. Acta* **68**, 4971–4992.

Shu, F.H., Shang, H., Lee, T., 1996. Toward an astrophysical theory of chondrites. *Science* **271**, 1545–1552.

Shu, F.H., Shang, H., Glassgold, A.E., Lee, T., 1997. X-rays and fluctuating x-winds from protostars. *Science* **277**, 1475–1479.

Thiemens, M.H., 1999. Mass-independent isotope effects in planetary atmospheres and the early Solar System. *Science* **283**, 341–345.

Umebayashi, T., 1983. The densities of charged particles in very dense interstellar clouds. *Prog. Theor. Phys.* **69**, 480–502.

Urey, H.C., 1947. The thermodynamic properties of isotopic substances. *J. Chem. Soc.*, 562–581.

Uyeda, C., Tsuchiyama, A., Okano, J., 1991. Magnesium isotopic fractionation of silicates produced in condensation experiments. *Earth Planet. Sci. Lett.* **107**, 138–147.

Wang, J., Davis, A.M., Clayton, R.N., Mayeda, T.K., Hashimoto, A., 2001. Chemical and isotopic fractionation during the evaporation of the FeO–MgO–SiO_2–CaO–Al_2O_3–TiO_2 rare earth element melt system. *Geochim. Cosmochim. Acta* **65**, 479–494.

Wark, D., Boynton, W.V., 2001. The formation of rims on calcium–aluminum-rich inclusions: Step I-Flash heating. *Meteor. Planet. Sci.* **36**, 1135–1166.

Wood, J.A., 2000. Pressure and temperature profiles in the Solar Nebula. *Space Sci. Rev.* **92**, 87–93.